

Surface modification of 316L stainless steel with magnetron sputtered TiN/VN nanoscale multilayers for bio implant applications

B. Subramanian · R. Ananthakumar ·
Akira Kobayashi · M. Jayachandran

Received: 1 August 2011 / Accepted: 11 November 2011 / Published online: 24 November 2011
© Springer Science+Business Media, LLC 2011

Abstract Nanoscale multilayered TiN/VN coatings were developed by reactive dc magnetron sputtering on 316L stainless steel substrates. The coatings showed a polycrystalline cubic structure with (111) preferential growth. XPS analysis indicated the presence of peaks corresponding to Ti2p, V2p, N1s, O1s, and C1s. Raman spectra exhibited the characteristic peaks in the acoustic range of 160–320 cm^{-1} and in the optic range between 480 and 695 cm^{-1} . Columnar structure of the coatings was observed from TEM analysis. The number of adherent platelets on the surface of the TiN/VN multilayer, VN, TiN single layer coating exhibit fewer aggregation and pseudopodium than on substrates. The wear resistance of the multilayer coatings increases obviously as a result of their high hardness. Tafel plots in simulated bodily fluid showed lower corrosion rate for the TiN/VN nanoscale multilayer coatings compared to single layer and bare 316L SS substrate.

1 Introduction

The latest trends of research in biomedical engineering centers are focused on problems connected with surface engineering of implants. Surface treatment methods that ensure minimal postoperative complications are developed. Biocompatibility of implants in tissue environment is

determined by inseparable biochemical, biomechanical, and bioelectronic factors. Biological reactions are analyzed with respect to metabolic, bacteriological, immunological, and oncological processes [1–5]. Medical grade 316L SS is presently being extensively used in medicine for implants. This grade of stainless steel has been used to avoid and/or minimize the pitting corrosion.

In recent years, various researchers have studied the application of protective coatings to orthopedic implants, e.g., hip prosthesis, in order to lengthen the utile life span by means of applying a thin film [6] or multilayers [7] with protective properties. Transition metal nitrides like TiN, VN, TiAlN, TaN, NbN, and ZrN, were successfully used as protective coatings against wear and corrosion in order to increase the life expectancy of surgical implants and prosthesis [8–11]. The coating should preferably have a high hardness value, corrosion resistance and resistance to mechanical wear, as well as biocompatibility and good adherence to the substrate on which they are deposited.

TiN is one of the most studied ceramic coatings due to its known biocompatibility [12]. This material leads to significant increase in the hardness of metallic surfaces, helps in protection against corrosion [13], and reduces bacterial colonization [14]. It is also responsible for a significant decrease in the metal ion release to the biological fluid [15]. TiN/NbN and TiN/VN multilayer coatings have shown interesting properties when compared to single layers of TiN, NbN, and VN in the form of enhanced hardness when deposited on single crystal substrates.

In this article we have investigated the materials properties of TiN/VN multilayered coatings on 316L stainless steel substrate. The role of multilayered coatings in improving the corrosion resistance in simulated bodily fluid, hemocompatibility, and bacterial attachment on coated stainless steel substrate was evaluated and discussed here.

B. Subramanian (✉) · R. Ananthakumar · M. Jayachandran
Central Electrochemical Research Institute, CSIR,
Karaikudi 630 006, India
e-mail: bsmanian@cecri.res.in

B. Subramanian · A. Kobayashi
Joining and Welding Research Institute, Osaka University,
Osaka 567-0047, Japan

2 Experimental methods

2.1 Preparation of magnetron sputtered TiN/VN multilayered coatings on 316L SS plates

TiN/VN multilayered coatings were prepared by reactive dc magnetron sputtering using 99.9% pure Titanium and Vanadium target. AISI 316L stainless steel substrates were cleaned in ultrasonic bath using acetone and trichloroethylene. After evacuating the chamber to a base pressure below 10^{-6} Torr, the substrate was cleaned by bombarding Ar^+ ions with a dc power of 150 W. The substrate temperature was kept at 400°C . The deposition parameters for TiN/VN sputtering are summarized in Table 1. The TiN and VN were deposited alternatively and the first layer was TiN and the last layer was VN. A single rotational substrate holder was used to obtain a layered structure. The total thickness of the coating was $1.7\ \mu\text{m}$. The total number of layers was about 150 with bilayer thickness of $90\ \text{Å}$. The total thickness of the coating was controlled by the deposition time.

2.2 Structural and compositional characterization

The structural analyzes of the textured coatings were carried out using an X-ray diffractometer. A Philips PANalytical X'pert PRO powder diffractometer system with $\text{Cu-K}\alpha$ radiation of wavelength $1.5418\ \text{Å}$ was used to study the phase evolution. The XRD system was operated at 20 kV and 10 mA in a 2θ range of $20\text{--}100^\circ$ using a step size of 0.02° and count time of 1 s. Raman spectra of the coatings was studied using Lab RAM—HORIBA Laser Raman Microscope with He–Ne laser. The data were collected with data point acquisition time of 10 s in the spectral region of $200\text{--}1200\ \text{cm}^{-1}$.

The surface microstructures of the specimens were studied using ERA-8800FE field emission scanning electron microscope (FESEM). The surface topography of the coatings was studied using Nano Navi atomic force microscopy (AFM). TEM analysis was studied using a

JEOL JEM-2100F field emission electron microscope. ImageJ software was used to analyze the SAED pattern. The chemical nature of the outermost part of TiN/VN multilayered coatings was obtained by X-ray photoelectron spectroscopy (XPS) techniques using Multilab 2000. Before making the measurement, the surface contamination was removed by sputtering with Ar ions.

2.3 Hemocompatibility and bacterial adhesion tests

In vitro platelet adhesion test was performed to investigate the quantity, morphology, aggregation, and pseudopodium of the adherent platelets. Platelet-rich plasma was prepared by centrifuging whole blood for 10 min at a rate of $1,000\ \text{rpm}\ \text{min}^{-1}$. Then it was dripped onto the sample surface and incubated for 60 min at 37°C . After incubation, PBS was used to remove the non-adherent platelets. The adhered platelets were fixed in 2.5% glutaraldehyde and critical point dried before gold sputtering and then the specimens were prepared for examination in the scanning electron microscope.

For the bacterial adhesion study, oral bacteria (*Bacillus megaterium* and *Bacillus pseudomycoides*) were isolated from orthodontic patients and identified by biochemical test and molecular identification (16S rRNA Gene Sequencing). 24 h young bacterial cultures were used for these experiments. The coated and uncoated specimens were immersed in separate 100 ml conical flasks that contained nutrient broth medium. Oral bacteria were inoculated in each nutrient broth medium and used as the experimental system while the un-inoculated specimen was used as the control system. The immersion period was 10 days. After immersion periods, coupons were removed from the medium. This specimen was used for fluorescence studies. The bacterial cells with poor adhesion were removed by washing with sterile distilled water. The coupons with biofilm were immersed for 20 min in a 3% glutaraldehyde solution in order to fix the biofilm to the steel surface. After that coupon was gently rinsed with autoclaved sterile distilled water and then three drops of 0.01% aqueous solution of acridine orange was added. It was incubated for 15 min; the excess stain was washed with autoclaved sterile distilled water and examined by the Epi-Fluorescence microscope E200, Nikon, Tokyo, Japan.

2.4 Mechanical test

Nanohardness and Young's modulus of the deposited layers were examined by means of a nanoindentation technique using nanoindenter (Nano Test) at a load of 5 mN using a Berkovich diamond indenter. Indentations were made on each sample at ten different locations and the values reported here represent the average of the ten readings.

Table 1 Deposition parameters for TiN/VN reactive sputtering

Objects	Specification
Target (2" Dia)	Ti (99.9%) & V (99.9%)
Substrate	AISI 316LSS
Target to substrate distance	60 mm
Ultimate vacuum	1×10^{-6} m bar
Operating vacuum	2×10^{-3} m bar
Sputtering gas (Ar:N_2)	2:1
Power	150 W
Substrate temperature	400°C

Wear resistance of the coated and uncoated substrates was examined by block on ring system. All the wear experiments were conducted at room temperature, ambient humidity, and without lubrication. A commercial grade steel ball bearing was used as the moving counterbody. The ring material, having a diameter of 60 mm, was made of high chromium high carbon tool steel with Vickers hardness 850 HV. The normal load was 400 g (3.924 N), with a sliding speed of 100 rev min⁻¹ and the sliding time was 2 min. The size of the samples was 3 × 1 cm. The friction coefficients were continuously recorded automatically. The wear rate was calculated by measuring the weight change of a specimen before and after the test.

2.5 Electrochemical corrosion behavior in simulated bodily fluid

To evaluate the corrosion behavior of the substrate and coatings, potentiodynamic polarization test, and electrochemical impedance spectroscopy (EIS) measurement were conducted in a test solution of modified Fusayama simulated bodily fluid [16]. Experiments were conducted using a standard three electrode configuration, with a platinum foil as the counter electrode, a saturated calomel electrode (SCE) as the reference electrode and the sample as the working electrode. The exposed surface area of all specimens was fixed at 1 cm² and the remaining portion except for the exposed area was painted with a strong adhesive silicon bond in order to prevent the initiation of crevice corrosion.

The potentiodynamic polarization test was carried out using Autolab PGSTAT12 system. The sample was kept in the solution for 60 min prior to the potentiodynamic polarization study in order to establish the open-circuit potential (E_{ocp}) or the steady state potential. After obtaining the stable open-circuit potential, the upper and the lower potential limits of linear sweep voltammetry were set at +200 and -200 mV, respectively, with respect to the E_{ocp} . The sweep rate was 1 mV s⁻¹. Porosity can indicate an obvious fracture path for adhesion failure. An empirical equation to evaluate the porosity (P) [17] of the coatings and protective efficiency is;

$$P = \frac{R_{ps}(\text{substrate})}{R_p(\text{coating/substrate})} 10^{-|\Delta E_{corr}/\beta_2|} \quad (1)$$

Here P is the total coating porosity, R_{ps} is the polarization resistance of the substrate material, R_p is the calculated polarization resistance of the coated system, and ΔE_{corr} is the potential difference between the bare substrate steel and the corrosion potentials of the coated steel and β_a is the anodic Tafel slope of the substrate. Calculated polarization resistance of the coated system is

$$R_p = \frac{(\beta_a \times \beta_c)}{\{2.3 \times i_{corr} \times (\beta_a + \beta_c)\}} \quad (2)$$

Here β_a is the anodic Tafel constant and β_c is the cathodic Tafel constant. Protective efficiency (P_i) [17] of the coating is determined from the polarization curve by below equation,

$$P_i = 100 \left(1 - \frac{i_{corr}}{i_{corr}^0} \right) \quad (3)$$

Here i_{corr} and i_{corr}^0 are the corrosion current densities in the presence and absence of the coating, respectively.

3 Results and discussion

3.1 Structural and compositional analysis

The X-ray diffraction pattern of TiN/VN nanoscale multilayer coatings prepared by reactive dc magnetron sputtering is shown in Fig. 1. The observed d values are in good agreement with the standard values with JCPDS card no 089-5265 for VN and 087-0633 for TiN coatings. They crystallized in cubic structure with lattice parameter of 4.16 Å and the peaks corresponding to (111), (200), (220), (311), and (222) planes were observed. The lattice parameter ‘ a ’ in case of cubic symmetry is calculated by using the formula [18],

$$\frac{1}{d^2} = \frac{1}{a^2[h^2 + k^2 + l^2]} \quad (4)$$

The crystallite size can be calculated using the Scherrer formula [18],

$$D_{hkl} = \frac{K\lambda}{\beta \cos \theta} \quad (5)$$

where D_{hkl} is the crystal size along the direction normal to the plane, K is Scherrer constant, $\lambda = 0.154$ nm and is the X-ray wavelength of Cu-K α radiation, β is the full-width at

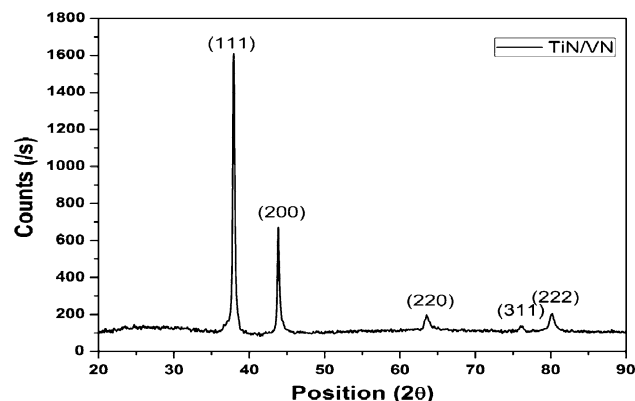


Fig. 1 XRD patterns of TiN/VN multilayers prepared by magnetron sputtering

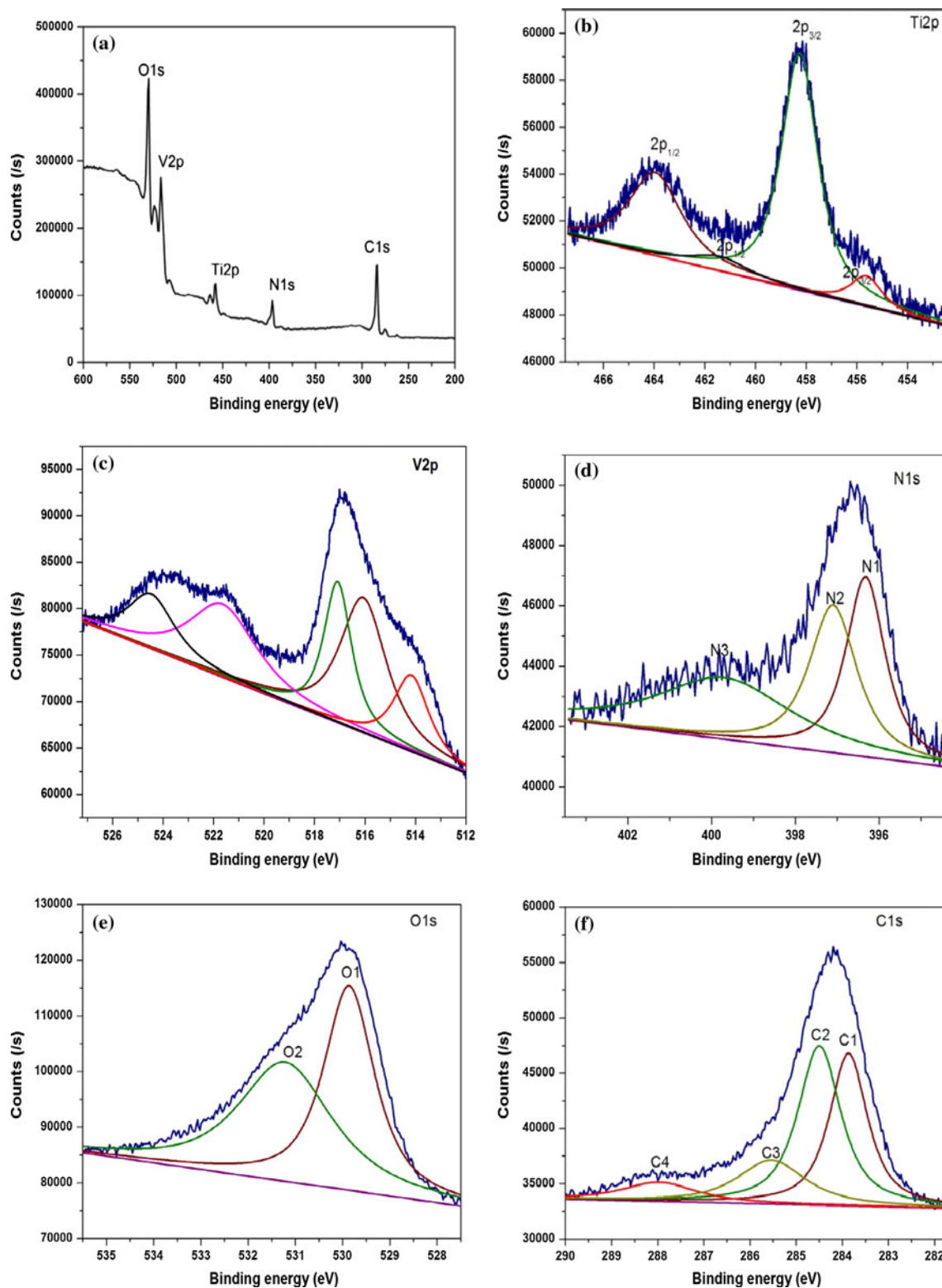


Fig. 2 XPS spectra of TiN/VN multilayer coatings deposited at 400°C **a** survey spectra, **b** Ti2p, **c** V2p, **d** N1 s, **e** O1 s and, **f** C1 s

half maximum of a Bragg peak; and θ is the Bragg angle. Calculation gave the values of the mean nanometer-scale crystallite-sizes of the film as 48 nm for the coatings. The

crystallite size reductions to the nanometer range results in considerable improvement in their resistance to localized corrosion [19].

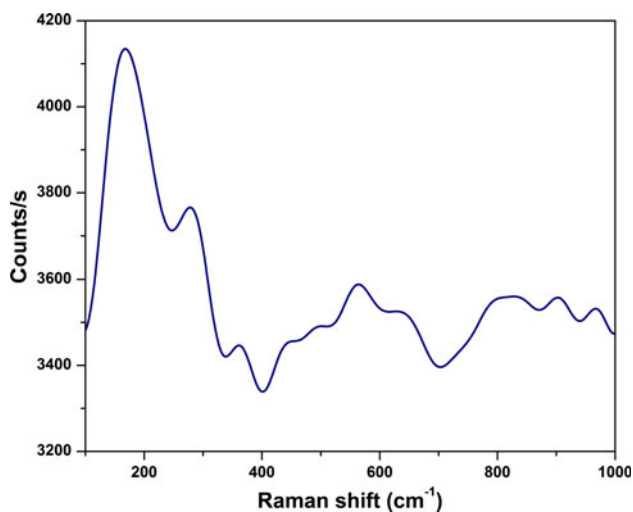


Fig. 3 The Raman spectra of TiN/VN multilayer coatings

The typical survey spectra of the TiN/VN nanoscale multilayer coatings are shown in Fig. 2a. The multilayer coatings exhibit the characteristic Ti2p, V2p, N1s, O1s, and C1s peaks at the corresponding binding energies 454.5, 516.1, 397.0, 530.6, and 284.1 eV, respectively [20]. For chemical state determination high resolution spectra of Ti2p, V2p, N1s, O1s, and C1s were recorded (Fig. 2b–f). The information on the chemical bonding states was obtained by subtracting the background with the linear method and deconvoluting the spectra by a curve-fitting method using a non-linear least squares fitting of a mixed Gaussian–Lorentzian product function.

Figure 2b shows high resolution spectra of Ti2p transition. The Ti2p photoelectron line is split into two components 2p3/2 and 2p1/2 according to split-orbit coupling. The position of Ti2p 3/2 for stoichiometric TiN falls in 455.6 eV and the peak found to 458.2 eV is identified as Ti⁴⁺ in a TiO₂ environment. The peaks appearing at 461.4 and 463.9 eV correspond to the 2p1/2 levels, of the Ti2p spin–orbit doublet characteristic of TiN and TiO₂ [21].

Figure 2c shows typical XPS spectra of the V2p doublet in TiN/VN multilayer coatings as a function of binding energy. The spectrum for the TiN/VN coatings in the V2p region showed the presence of two well resolved spectral lines at 514.2 and 521.6 eV [22]. These were assigned to the V2p3/2 (at 514.2 eV) and V2p1/2 (at 520.9 eV) spin orbit component for VN, respectively. The peak appearing at 516.2 eV (2p3/2) is due to the formation of V₂O₃. The other two peaks at 524.4 (2p1/2) and 517.1 eV (2p3/2) are due to the formation of V₂O₃ and V₂O₅ [22].

The N1s spectra recorded from the samples showed (Fig. 2d) the presence of these contributions: N1, N2, and N3, with corresponding binding energies. The contribution,

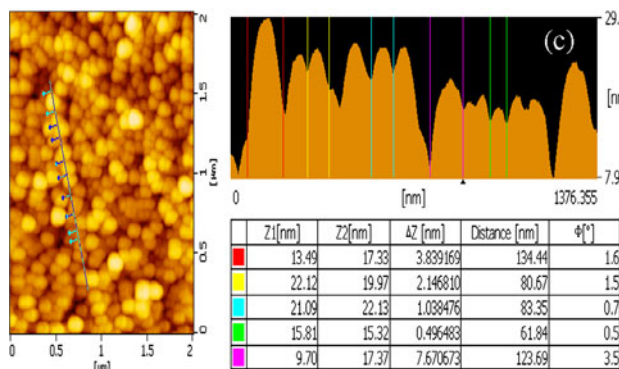
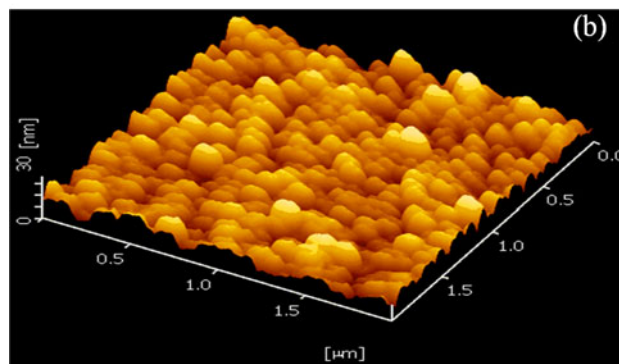
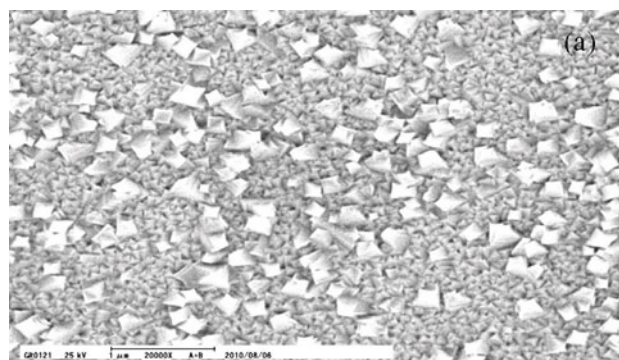


Fig. 4 a SEM image of the TiN/VNcoatings, b AFM 3D image, and c AFM 2D image of the multilayer coatings

N1 located at 396.3 eV corresponds to Ti–N bonding in TiN. The peak at 397.0 eV (N2) is characteristic for VN. The broad contribution, N3, appearing at binding energy (399.6 eV) has been commonly assigned to Ti oxynitrides of the type TiO_xN_y [22].

The O1s spectra contained two contributions (Fig. 2e). The main one located at 529.8 eV, corresponds to Ti–O bonds. The assignment of the second oxygen contribution positioned at 531.2 eV has been attributed to V₂O₅ and OH groups [22].

Figure 2f shows the C1s spectrum for the multilayer coatings which consists of four deconvoluted components. The main component at 283.8 (C1) and 284.6 (C2) corresponds to C–H bonding, while the smaller components at 285.6 eV (C3) is associated to C–N and C–H bond and

Fig. 5 **a** Cross sectional TEM image and **b** SAED pattern for TiN/VN multilayer coatings

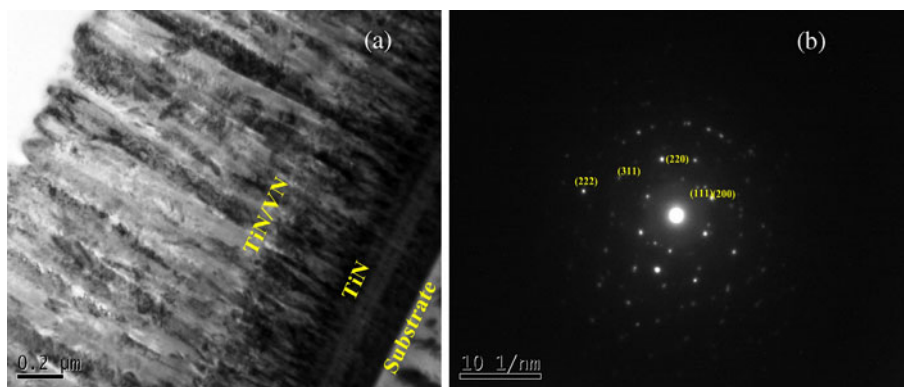
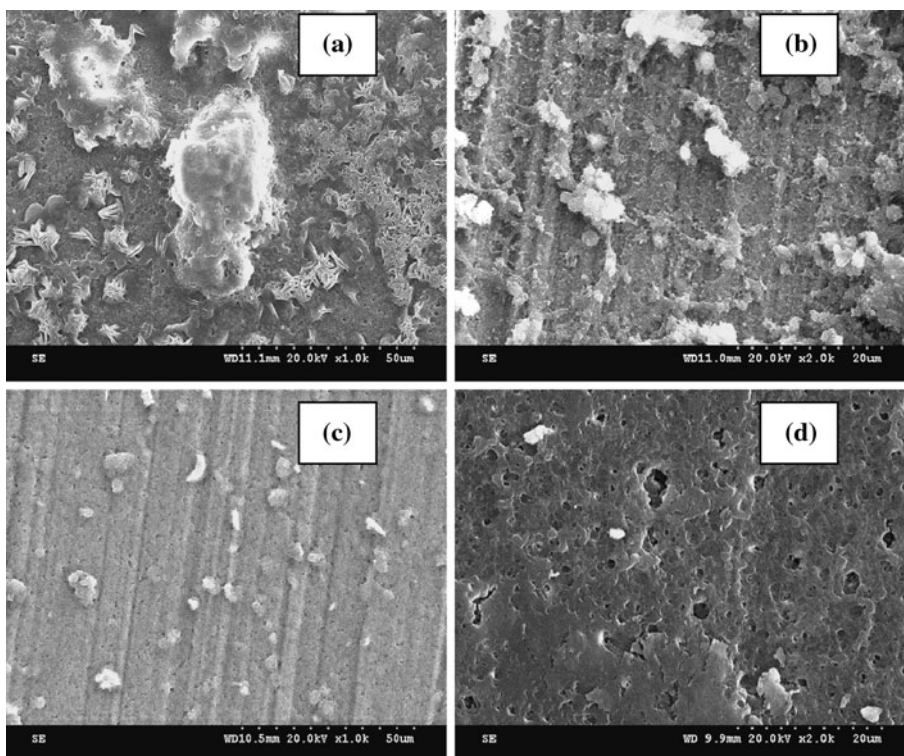


Fig. 6 Morphology of platelet adherent on **a** steel substrate, **b** TiN, **c** VN, and **d** TiN/VN multilayers



component at 287.9 eV (C4) is to C=O bond and they all originate from atmospheric contamination [23].

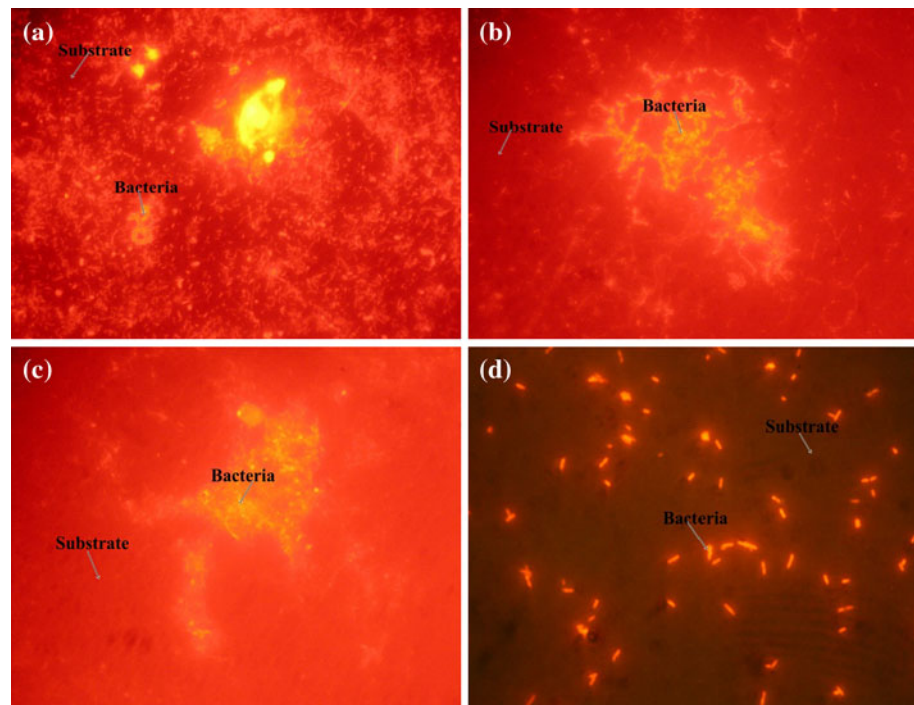
Figure 3 shows the Raman spectra of DC magnetron sputtered TiN/VN nanoscale multilayers. The TiN/VN multilayer coating shows both an acoustic band at 200–400 cm^{-1} and an optical band at 550–700 cm^{-1} . For transition metal nitrides, Raman spectroscopy detects distortions induced by vacancies, including an acoustic band induced by metal ions and an optical band by non-metal ions [24]. The characteristic peaks at 278 cm^{-1} are due to the formation of transverse acoustic (TA)/longitudinal acoustic (LA) mode and 638 cm^{-1} is related to transverse optical (TO)/longitudinal optical (LO) mode and 445 cm^{-1} peak corresponds to the second-order acoustic (2A) modes of VN. The peaks at 166, 360, 490, 565, and 830 cm^{-1} , related to TA/LA, 2A, TO and

acoustic/optic (A + O) modes of TiN [24], respectively, were observed in the Raman spectra of TiN films. This result confirms the successful formation of TiN/VN nanoscale multilayered film.

3.2 Morphological studies

Scanning electron microscope image of the coatings showed (Fig. 4a) that the particles are agglomerated and grain size is about 20–30 nm. AFM image of the TiN/VN multilayer coatings showed (Fig. 4b, c) dense microstructure. The average grain size measured of these formations is about 20–30 nm as shown in Fig. 4c using particle analysis and section analysis tools. The average height of this formation is 20 nm and the root mean square surface roughness of the coatings is 5.4 nm.

Fig. 7 Bacterial adhesion image on **a** steel substrate, **b** TiN film, **c** VN film, and **d** TiN/VN multilayered film



The bright field TEM micrograph of the cross section of the TiN/VN multilayer coatings is shown in Fig. 5a. The section comprises of the steel substrate, base layer (TiN) and columnar TiN/VN multilayer coating. There is no evidence of significant microstructural changes either in the coating or in the substrate. The excellent bond between coating and substrate and the columnar structure of the coating were observed. The polycrystalline diffraction pattern (Fig. 5b) confirms the information provided by X-ray diffraction. The nature of crystallinity was further examined by using selected area electron diffraction (SAED), conventional TEM techniques. The SAED pattern showed a spotty-discontinuous ring pattern in Fig. 5b. The rings marked 1–5 match with (111), (200), (220), (311), and (222) planes of TiN phase.

3.3 Platelet adhesion test

Figure 6 shows the morphology of the platelets adhering to the TiN/VN nanoscale multilayer, VN, TiN single layer coatings and on AISI 316LS substrates after incubation for 60 min. The number of adherent platelets on the surface of the TiN/VN multilayer, VN, TiN single layer coating exhibit fewer aggregation and pseudopodium compared to AISI 316LS substrates. Figure 6 also indicates that adherent platelets on the TiN/VN multilayer coatings are even lesser than those on the single layer VN and TiN coatings. Our experiments demonstrate that the scalar and active levels of adhered platelets on coated samples are lower than those on stainless steel substrate. Here, denaturing and

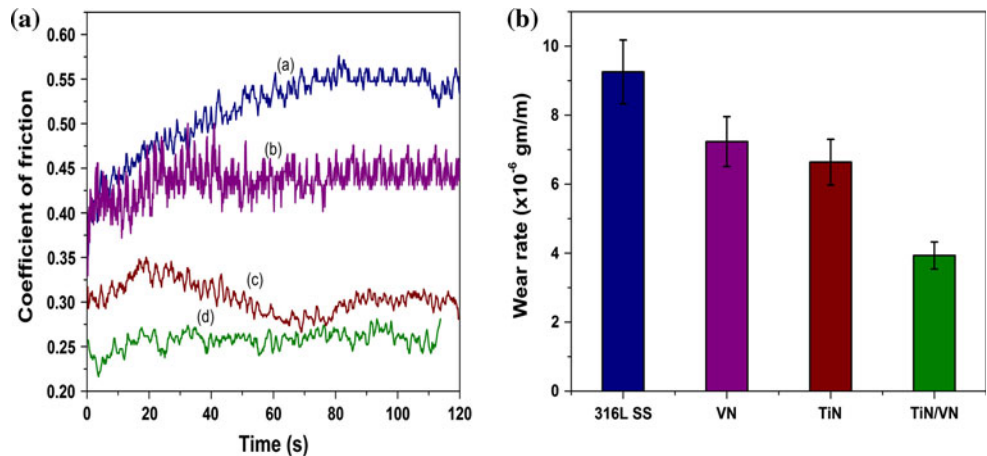
aggregation of the platelets are observed to be impeded, and platelet adhesion is also reduced on the coated surface.

3.4 Bacterial attachment studies

Figure 7 shows the typical epi-fluorescence microscope images of the TiN/VN multilayer, TiN, VN single layer coatings and bare AISI 316L stainless steel substrates after bacterial adhesions test. Bacterial adherence to the implant surface is considered to be an important event in the pathogenesis of bacterial infections and implant failure. This adherence is associated with the development of inflammation of the peri-implant soft tissues, crestal bone loss, and peri-implant pathology. The initial, nonspecific adherence is thought to involve nonspecific processes mediated by physico-chemical interactions such as hydrophobic interactions and electrostatic interactions [25]. The specific adherence is mediated by extracellular polysaccharides and lectin-like substances [26]. In the oral cavity, teeth and dental implant surfaces (transgingival abutment or healing implant components) are covered by an acquired pellicle formed by adsorption of salivary components to the surface of the teeth, implants, and restorations. Oral bacteria must then interact with these salivary components in order to adhere to the surface. A correlation between plaque accumulation and progressive bone loss around implants has been reported in experimental and clinical studies [27].

The results of the present study show that the implants coated with TiN/VN multilayer presented a minor quantity

Fig. 8 **a** Variation of friction coefficient with sliding time and **b** wear rate of steel ring after sliding against steel substrate, VN, TiN, and TiN/VN



of the surface covered by bacteria. The attached bacteria were higher on uncoated substrates with higher roughness than on coated substrates. As bacteria accumulated on the uncoated 316L stainless steel, they exhibited typical phenotypic properties of biofilm formation. Rough surface is one of the requirements for improved cell attachment and integration [28]. Visual observation showed that TiN and VN single layer coatings had lesser bacterial cells compared to the substrate. Of all the coatings, the attachment of bacteria on TiN/VN multilayer coatings was found to be very minimum and without colonization because the multilayer coating surface had very smooth surface. Also, the film composition would have been responsible for the large variation in bacterial adhesion as it would have mediated the bacterial adhesion through charge transfer interactions.

3.5 Mechanical studies

Nanohardness of TiN, VN monolayer, and TiN/VN multilayers was determined on the coated steel substrate by using a nanoindenter. The nanohardness and young's modulus of the TiN/VN multilayer coating, calculated from this plot, was about 30.04 and 186.99 GPa. Monolayer layer TiN and VN showed hardness of about 23.67 and 20.67 GPa and young's modulus of 184.64 and 179.89 GPa, respectively. The hardness of multilayers is thus very high as compared to the monolayers.

The friction coefficient of 316LSS, TiN, VN single layer, and TiN/VN multilayer coatings, which were prepared by reactive dc magnetron sputtering method, evaluated against steel ball as a counter material is shown in Fig. 8a. 316LSS, TiN, and VN single layer coatings showed average friction coefficients of 0.52, 0.45, and 0.31, respectively, the TiN/VN multilayer coatings showed the lowest friction coefficient of 0.25 among them. The lower friction coefficient observed in Fig. 8a for the TiN/VN on 316LSS indicates that this stack has better wear resistance.

Figure 8b shows the comparative diagram of wear rates of TiN/VN multilayer coatings with TiN, VN single layer and bare substrate. The wear rates for TiN/VN coatings are 3.93×10^{-6} gm m^{-1} . As can be seen in the diagram, the wear rate of TiN/VN coatings is significantly lower than that of TiN (6.63×10^{-6} gm m^{-1}), VN (7.23×10^{-6} gm m^{-1}) and bare substrate (9.25×10^{-6} gm m^{-1}). Experimental data clearly indicates that TiN/VN multilayer coating has superior wear resistance compared to single layer and bare substrate. Generally the wear resistance of a material has been directly related to its hardness, i.e., the higher the hardness higher the wear resistance.

3.6 Polarization studies

AISI316L stainless steel has been widely used for biomedical implants, such as orthopedic, cardiovascular, and dental devices. The success of implants in the human body depends on their biosafety, biocompatibility, and biofunctionality in

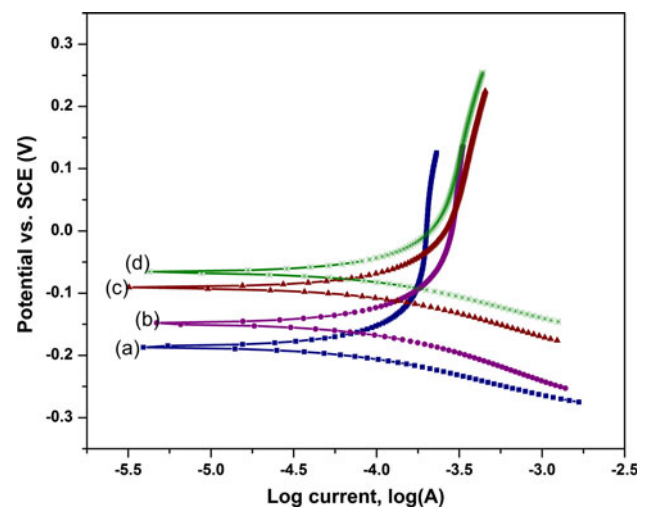


Fig. 9 Polarization studies of **a** steel substrate, **b** TiN film, **c** VN film, and **d** TiN/VN multilayered film in simulated bodily fluid

Table 2 Potentiodynamic polarization data obtained from Tafel plots

Sample	E_{corr} V	$I_{\text{cor}} \times 10^{-5} \text{ A cm}^{-2}$	Corrosion rate mpy	$R_p \text{ } \Omega \text{ cm}^2$	Porosity	Protective efficiency (%)
AISI 316L SS	−0.186	3.34	1.25	797.18	–	–
VN	−0.149	1.24	0.46	2110.70	0.1971	62.8
TiN	−0.091	1.01	0.37	2768.15	0.0542	69.7
TiN/VN	−0.066	0.66	0.25	4969.77	0.0194	80.2

the environment where implants are placed in. With the aim of studying the protection abilities and stabilities on localized corrosion of coating, potentiodynamic polarization measurements were carried out in simulated body fluid conditions.

The potentiodynamic polarization curves for the TiN/VN multilayer, VN, TiN single layer coatings and bare substrate are shown in Fig. 9 and the measured corrosion potential (E_{corr}) calculated from the intersection of the Tafel slopes, corrosion current density (i_{corr}) which was also obtained from the intersection of the Tafel slopes and corrosion rate, polarization resistance, protective efficiency (Pi), and porosity (P) are given in Table 2. The coated samples show a positive shift in corrosion potential, when compared to bare substrate. The corrosion current is observed to be minimum at $0.51 \times 10^{-5} \text{ A/cm}^2$ for the TiN/VN on AISI 316L substrate stack as evident from Table 2. There is an appreciable increase in corrosion resistance for the TiN/VN multilayer coated substrate compared to TiN, VN, and bare AISI substrate. It clearly shows that passive film is formed on the TiN/VN multilayer coated substrate and demonstrates good corrosion resistance of the multilayer coated specimens because passivity formation in multilayer coatings can be interpreted using wide passive potential range and low current density. The electrochemical determination gives a porosity of 0.0194 for the TiN/VN multilayer coatings, 0.0542 for TiN single layer coating and 0.0194 for VN single layer coating. Porosity of the multilayer coatings showed lower value than that of other coatings. The corrosion current density indicates the protective efficiency. The highest protective efficiency was 80.2% for the TiN/VN multilayer coatings which was well passivated, with a wide passive potential range and low passive current density compared to the single layer coatings and bare substrate. This protective efficiency is related to crack formation, spallations of the film and porosity in coatings. This suggests that significant improvement in corrosion resistance in human body environment can be achieved, by TiN/VN multilayer coatings.

4 Conclusions

Nanoscale TiN/VN multilayers were successfully deposited on 316L stainless steel substrates by reactive dc

magnetron sputtering. X-ray diffraction analysis reveals that the films are polycrystalline in nature with face centered cubic structure for nanoscale TiN/VN multilayered coatings. These coatings were characterized using Raman microscopy to elucidate the behavior of the optic and acoustic phonon modes of the crystalline lattices. The presence of different phases like TiN, TiO_2 , VN, V_2O_3 , and V_2O_5 was identified by XPS analysis. TiN/VN multilayer coatings had better hemocompatibility than TiN, VN single layer, and bare AISI 316L SS substrates. The attachment of bacteria on TiN/VN multilayer coatings was found to be very minimum and without colonization. The wear resistance of TiN/VN multilayer coatings shows more improvement than that of the single layer and bare substrate, which is correlated with their high hardness. A significant improvement in corrosion resistance in human body environment could be achieved by TiN/VN multilayer coatings on 316L stainless steel substrates. The TiN/VN multilayer coated samples show better protective efficiency than the single layer and uncoated samples.

Acknowledgements One of the authors (B.S) thanks the Department of Science & Technology, New Delhi, for a research grant under SERC scheme No. SR/S1/PC/31/2008 and the Japan Society for the Promotion of Science, Japan for the award of FY 2011 JSPS Long term Invitation fellowship. We thank Prof. M.Takahashi and H.Nishikawa of JWRI, Osaka University, Japan for the HRTEM and nanoindentation analyzes and Dr S. Maruthamuthu, Biocorrosion Division of Central Electrochemical Research Institute, Karaikudi, India for the Epi-fluorescence studies.

References

1. Kajzer W, Kaczmarek M, Krauze A, Marciniak J. Surface modification and corrosion resistance of Ni–Ti alloy used for urological stents. *J Achieve Mater Manufact Eng.* 2007;20:123–6.
2. Kajzer W, Krauze A, Walke W, Marciniak J. Corrosion resistance of Cr–Ni–Mo steel in simulated body fluids. *J Achieve Mater Manufact Eng.* 2006;18:115–8.
3. Kajzer W, Kaczmarek M, Marciniak J. Biomechanical analysis of stent–oesophagus system. *J Mater Process Technol.* 2005; 162–163:196–202.
4. Krauze A, Zi bowicz A, Marciniak J. Corrosion resistance of intramedullary nails used in elastic osteosynthesis of children. *J Mater Process Technol.* 2005;162–163:209–14.
5. Marciniak J. Perspectives of employing of the metallic biomaterials in the reconstruction surgery. *Eng Biomater.* 1997;1: 12–20.

6. Günzel R, Mandl S, Richter E, Liu A, Tang BY, Chu PK. Corrosion protection of titanium by deposition of niobium thin films. *Surf Coat Technol.* 1999;116–119:1107–10.
7. Hübler R. Characterisation of gradient interfaces in thin film multilayers used to protect orthopaedic implants. *Surf Coat Technol.* 1999;116–119:1116–22.
8. Braic M, Balaceanu M, Braic V, Vladescu A, Pavelescu G, Albulescu M. Synthesis and characterization of TiN, TiAlN and TiN/TiAlN biocompatible coatings. *Surf Coat Technol.* 2005;200:1014–7.
9. Hqbler R, Schrfel A, Ensinger W, Wolf GK, Schreiner WH, Baumvol IJR. Plasma and ion-beam-assisted deposition of multilayers for tribological and corrosion protection. *Surf Coat Technol.* 1993;60:561–5.
10. Leng YX, Sun H, Yang P, Chen JY, Wang J, Wan GJ, Huang N, Tian XB, Wang LP, Chu PK. Biomedical properties of tantalum nitride films synthesized by reactive magnetron sputtering. *Thin Solid Films.* 2001;398–399:471–5.
11. Hqbler R, Cozza A, Marcondes TL, Souza RB, Fiori RF. Wear and corrosion protection of 316-L femoral implants by deposition of thin films. *Surf Coat Technol.* 2001;142–144:1078–83.
12. Narayan J, Fan WD, Narayan RJ, Tiwari P, Stadelmaier HH. Diamond, diamond-like and titanium nitride biocompatible coatings for human-body parts. *Mater Sci Eng B.* 1994;25:5–10.
13. Raimondi MT, Pietrabissa R. The in vivo wear performance of prosthetic femoral heads with titanium nitride coating. *Biomaterials.* 2000;21:907–13.
14. Groessner-Schreiber B, Neubert A, Muller WD, Hopp M, Griepentrog M, Lange KP. Fibroblast growth on surface-modified dental implants: an in vitro study. *J Biomed Mater Res A.* 2003;64A:591–9.
15. Fisher J, Hu XQ, Stewart TD, Williams S, Tipper JL, Ingham E, Stone MH, Davies C, Hatto P, Bolton J, Riley M, Hardaker C, Isaac GH, Berry G. Wear of surface engineered metal-on-metal hip prostheses. *J Mater Sci Mater Med.* 2004;15(3):225–35.
16. Huang HH, Hsu CH, Pan SJ, He JL, Chen CC, Lee TL. Corrosion and cell adhesion behavior of TiN-coated and ion-nitrided titanium for dental applications. *Appl Surf Sci.* 2005;244:252–6.
17. Ananthakumar R, Subramanian B, Jayachandran M. Electrochemical corrosion and materials properties of reactively sputtered TiN/TiAlN multilayer coatings. *Ceramic Inter.* 2011 (Inpress).
18. Subramanian B, Ananthakumar R, Vidhya VS, Jayachandran M. Influence of substrate temperature on the materials properties of reactive DC magnetron sputtered Ti/TiN multilayered thin films. *Mater Sci Eng B.* 2011;176(1):1–7.
19. Mu H, Seok J, Lin RY. Nickel thin film coatings on steels with electroless plating and sputtered deposition. *J Electrochem Soc.* 2003;150(2):c67–72.
20. Zhao J, Garza EG, Lam K, Jones CM. Comparison study of physical vapor-deposited and chemical vapor-deposited titanium nitride thin films using X-ray photoelectron spectroscopy. *Appl Surf Sci.* 2000;158:246–51.
21. Halbritter J, Leiste H, Mathes HJ, Walk P. Fresenius: AR-XPS: studies of nucleation and make-up of sputtered TiN-layers. *J Anal Chem.* 1991;341:320–4.
22. Glaser A, Surnev S, Netzer FP, Fateh N, Fontalvo GA, Mitterer C. Oxidation of vanadium nitride and titanium nitride coatings. *Surf Sci.* 2007;601:1153–9.
23. Beguin F, Rashkov I, Manolova N, Benoit R, Erre R, Delpoux S. Fullerene core star-like polymers-1. Preparation from fullerenes and monoazidopolyethers. *Eur Poly J.* 1998;34(7):905–15.
24. Constable CP, Yarwood J, Munz WD. Raman microscopic studies of PVD hard coatings. *Surf Coat Technol.* 1999;116–119:155–9.
25. O'Brien NJ, Fan PL, Loesche WJ, Walker ML, Apostolid A. Adsorption of streptococcus mutans on chemically treated hydroxyapatite. *J Dent Res.* 1978;2:910–4.
26. Schilling KM, Bowen WH. Glucans synthesized in situ in experimental salivary pellicle function as specific binding sites for streptococcus mutans. *Infect Immun.* 1992;60:284–94.
27. Lindhe J, Berglundh T, Ericsson I, Liljenberg B, Marinello C. Experimental breakdown of peri-implant and periodontal tissues. A study in the beagle dog. *Clin Oral Implant Res.* 1992;3:9–16.
28. Jayachandran YL, Venkatachalam S, Karunakaran B, Narayandass SaK, Mangalaraj D, Bao CY, Zhang CL. Bacterial adhesion studies on titanium, titanium nitride and modified hydroxyapatite thin films. *Mater Sci Eng C.* 2007;27:35–41.